Dynamics of biofilm processes

Authors: Michael Gerald Trulear and William G. Characklis

This is a postprint of an article that originally appeared in Proceedings of the 34th Industrial Waste Conference in 1979.

Trulear, M.G. and W.G. Characklis, "Dynamics of Biofilm Processes," Proceedings of the 34th Industrial Waste Conference, Purdue University, 1979, pp. 838-853.

79-001

40

"Dynamics of Biofilm Processes"

by

M. G. Trulear, Graduate Student
W. G. Characklis, Professor

George R. Brown School of Engineering
Rice University
Houston, Texas 77001

Presented at the 34th Annual Purdue INDUSTRIAL WASTE CONFERENCE,
West Lafayette, Indiana May 8-10, 1979

INTRODUCTION

The term fouling refers to the formation of inorganic and/or organic deposits on surfaces. In cooling systems, these deposits form on condenser tube walls increasing fluid frictional resistance, accelerating corrosion and impairing heat transfer. Biological fouling, or biofouling, results from the attachment and growth of microbial organisms.

The Problem

The most common method for controlling fouling biofilm development is periodic chlorination. Recently, concern over residual toxicity from hypochlorous acid and its reaction products has resulted in federal regulations which limit the allowable chlorine concentration in cooling water discharges. This investigation stems from the apparent need for a better basic understanding of fouling biofilm development and fouling biofilm destruction so that the impact of these new regulations on power plant operations can be evaluated.

Processes Contributing to Biofilm Development

Based on experimental observation in this research, biofilm development on a surface exposed to fluid flow is the net result of physical transport and biological growth rate processes. The processes which contribute to the overall biofilm accumulation are:

- organic adsorption
- transport of microbial particles to the surface
- microorganism attachment to the surface
- growth of attached microorganisms
- reentrainment of biofilm by fluid shear

The adsorption of an organic monolayer occurs within minutes after exposure of an initially "clean" surface to a flowing fluid which contains

dispersed microorganisms, nutrients, and organic molecules. Baier[2,3,4,5] has investigated the dynamics of this organic adsorption and suggests that it is a prerequisite for biological attachment because it conditions the surface.

The transport of microbial particles from the bulk to the surface depends on the fluid flow regime. In turbulent flow, molecular diffusion and turbulent eddy transport are viable mechanisms. In a quiescent fluid, chemotaxis is possible.

Numerous mechanisms have been postulated for the process of microbial attachment to the surface.[11,18] Most agree that the production of a polysaccharide binding material is necessary.

Biofilm growth is considered as the combined effect of cellular reproduction and exopolysaccharide production. Numerous investigators[1,8,9,10] have postulated equations which describe the rate of substrate removal as a function of limiting nutrient concentration and biofilm mass. The biological rate equations presented by Atkinson[1] also account for the fundamental process of substrate diffusion into the biofilm matrix. Few studies have attempted to relate substrate removal rate to biofilm development rate.

At any point in the development of a biofilm, portions of biofilm are sheared away and reentrained in the fluid flow. Reentrainment is highly dependent on hydrodynamic conditions. In addition to shearing, sloughing can also significantly contribute to reentrainment. Sloughing refers to a random, massive removal of biofilm attributed to oxygen/nutrient depletion deep within biofilms. Sloughing is more frequently witnessed with thicker, less dense films which develop under low fluid shear conditions.

Biofilm accumulation is the net result of all these rate processes occurring simultaneously (Fig. 1). At specific times in the overall biofilm development, certain processes contribute more than others.

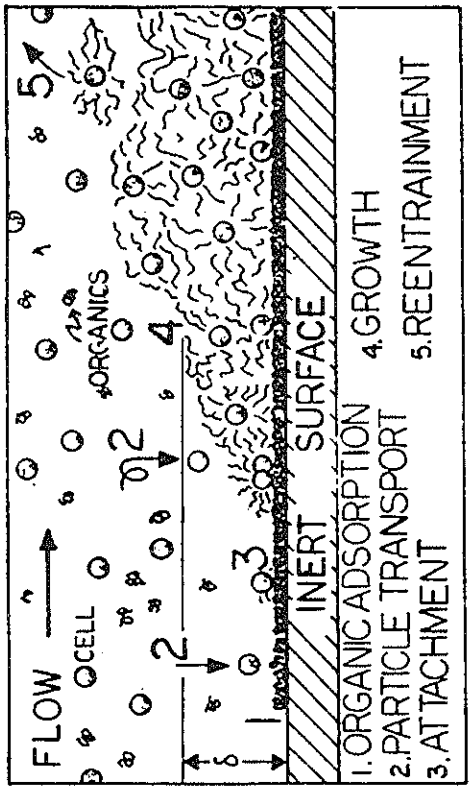

Figure 1. Processes Contributing to Biofilm Development

EXPERIMENTAL APPARATUS AND METHODS

Two laboratory reactor configurations were used in this study:

1. a tubular reactor (Fig. 2)
2. an annular reactor consisting of a stationary outer cylinder and a rotating inner cylinder (Fig. 3)

The tubular geometry is identical to the prevalent geometry in power plant condensers. The annular reactor was tested as a biofouling monitor because its response (in terms of fluid frictional resistance) is very sensitive to fouling, and the reactor system is easy to operate and maintain.

Biofilm accumulation was measured directly by determining biofilm thickness and/or attached biomass. Biofouling was observed indirectly by measuring changes in fluid frictional resistance or heat transfer resistance. In the tubular reactor systems, fluid frictional resistance was determined by pressure drop measurements using an inclined mercury manometer. A torque monitor connected to the inner cylinder measured fluid frictional resistance in the annular reactor system.

Nutrients, glucose and in some cases, a synthetic growth media, were added to the reactor systems to provide the necessary mineral, energy and carbon requirements for microbial growth. The feed water to the experimental reactors was tap water which had been treated to remove residual suspended solids and chlorine.

The experiments were initiated by inoculating with a mixed population of microorganisms and operating the reactors in a batch mode (as opposed to continuous flow) until some surface colonization occurred (usually 6-8 hours). This technique minimizes the induction period (Fig. 4) which may last for weeks under some of the conditions tested.

Further details concerning methods and apparatus can be found elsewhere.[6,14,17]

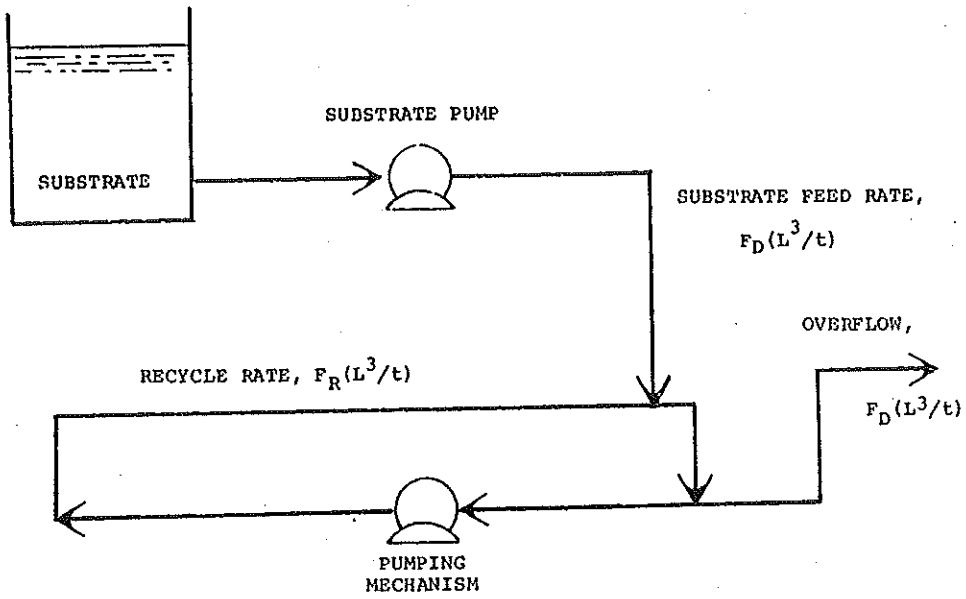

Figure 2. Schematic Diagram of Tubular Reactor System

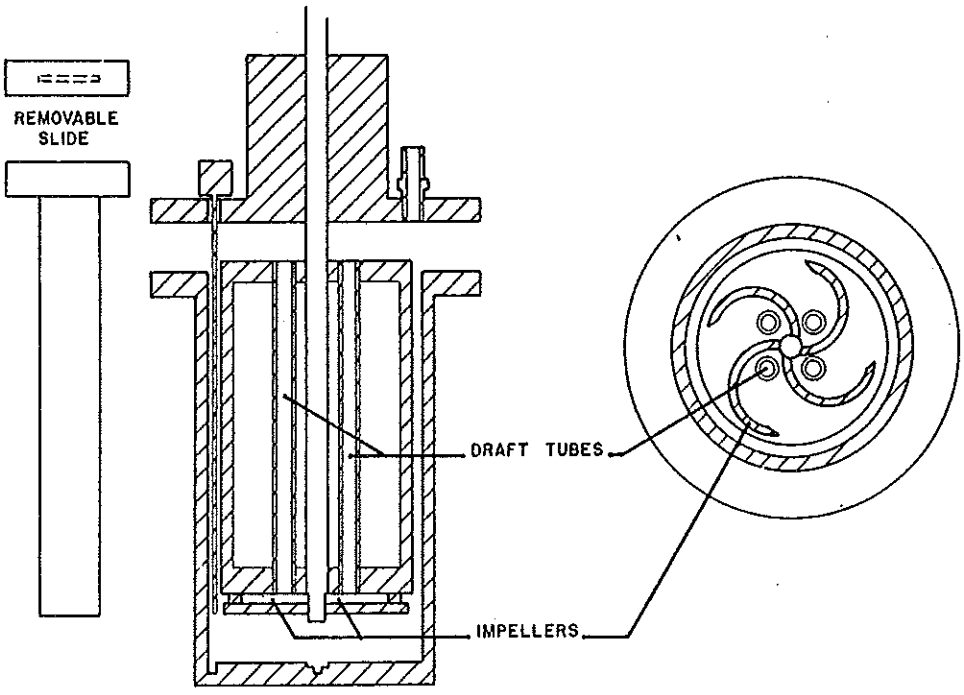

Figure 3. Schematic Diagram of Annular Reactor

RESULTS AND DISCUSSION

The overall process of biofilm development can be conveniently divided into three phases:

- induction
- growth
- plateau

These phases are indicated in Figure 4.

The induction phase is characterized by the development of a primary layer of biofilm on an initially "clean" surface. Organic adsorption, followed by the transport and attachment of microorganisms to the surface are significant rate processes during the induction period.

The induction period is followed by a growth phase. The growth phase is characterized by two stages of accumulation, a logarithmic increase followed by a near constant accumulation rate. The logarithmic portion begins in the latter stages of the induction period and continues until a "critical" film thickness is attained. At the critical thickness, substrate utilization reaches a steady-state value, and is not affected by additional film accumulation. A period of near constant accumulation is then observed which is terminated when the shearing of the biofilm prevents further accumulation.

The last period is the plateau phase in which new biofilm growth equals the biofilm being sheared from the surface by the fluid. Hence, during the plateau phase, biofilm thickness remains essentially constant.

The suspended biomass concentration increases proportionally with biofilm thickness. In the biofilm reactors used for this study, the influent suspended biomass concentration was zero. Furthermore, the reactors were operated at hydraulic detention times of 15 minutes or less so that biomass production due to growth processes would be limited to the attached biomass.

Hence the increase in suspended solids with time can be directly attributed to the process of biofilm reentrainment.

System Material Balances

The material balance approach is useful to account for the removal of substrate from the bulk fluid, the production of attached biomass and reentrainment of biomass from the surface. A mass balance on substrate across the system yields the following:

$$V \frac{dS}{dt} = F(S_i - S) - \frac{R_g}{Y} - \frac{R'_g}{Y'} \qquad (1)$$

where

V =	volume of liquid solution	(L^3)
S =	substrate concentration in the solution	(ML^{-3})
t =	time	(t)
F =	volumetric flow rate of the liquid	(L^3t^{-1})
S_i =	influent substrate concentration	(ML^{-3})
R_g =	attached biomass growth rate	(Mt^{-1})
Y =	attached biomass yield coefficient	(dimensionless)
R'_g =	suspended biomass growth rate	(Mt^{-1})
Y' =	suspended biomass yield coefficient	(dimensionless)

The removal of substrate due to suspended biomass growth is negligible in comparison to substrate consumption for attached biomass growth. Neglecting the substrate removal term for suspended biomass growth, Eq. (1) may be rewritten as:

$$V \frac{dS}{dt} = F(S_i - S) - \frac{R_g}{Y} \qquad (2)$$

An inventory of the total biomass in the system is as follows:

$$M_T = A\rho Th + VX \qquad (3)$$

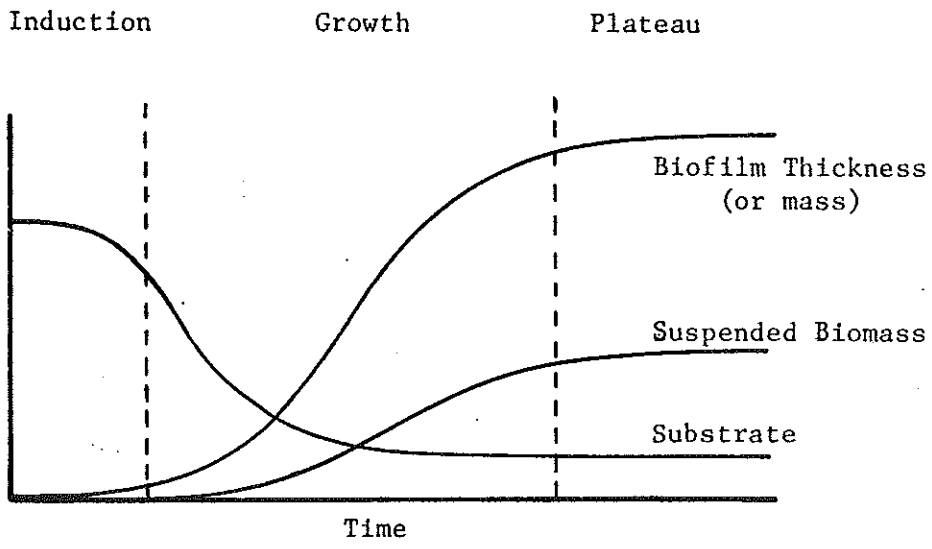

Figure 4. Typical Experimental Progression

where M_T = total system biomass (M)

A = reactor surface area (L^2)

ρ = biofilm volumetric density (ML^{-3})

Th = biofilm thickness (L)

X = suspended biomass concentration in the bulk solution (ML^{-3})

For constant V, A, and ρ, the change in total mass with time is:

$$\frac{dM_T}{dt} = A\rho \frac{dTh}{dt} + V \frac{dX}{dt} \quad (4)$$

where $A\rho \frac{dTh}{dt}$ and $V \frac{dX}{dt}$ represent the net accumulation of attached and suspended biomass. Although biofilm density is essentially constant during a given experiment, between experiments it varies with influent substrate concentration (Fig. 5) and fluid shear stress at the wall.[17]

The accumulation of attached biomass will be considered the net result of two individual processes: biofilm growth and biofilm shearing. The rate of biofilm growth, R_g, is related to the rate of substrate removal and was previously defined in Eq. (1). The net accumulation of attached biomass can then be written as follows:

$$A\rho \frac{dTh}{dt} = R_g - R_s \quad (5)$$

where R_s is the biofilm shearing rate (Mt^{-1}).

The net accumulation of suspended biomass can be expressed by the following material balance:

$$V \frac{dX}{dt} = F(X_i - X) + R_s + R'_g \quad (6)$$

where X_i is the influent suspended biomass concentration (ML^{-3}). Since the influent suspended biomass concentration was zero in this study and the production of suspended biomass due to dispersed growth is assumed negligible,

Eq. 6 can be rewritten as follows:

$$V \frac{dX}{dt} = -FX + R_s \quad (7)$$

The substrate removal rate $\frac{R_g}{Y}$, the biofilm growth rate, R_g, and the biofilm shearing rate, R_s, are the process rates of concern since they determine the rate of biofilm development. The next sections will discuss each process rate in somewhat more detail.

Substrate Removal Rate

The substrate removal rate increases in proportion to biofilm thickness up to a critical thickness beyond which removal rate remains constant (Fig. 6). The critical thickness is observed to increase with influent substrate concentration. This behavior is confirmed by other investigators[9,10,17] and is attributed to nutrient diffusional limitations within the biofilm. Once the biofilm thickness exceeds the depth of substrate or oxygen penetration into the biofilm (Fig. 7), the removal rate is unaffected by further biofilm accumulation.

The substrate removal rate is also dependent on fluid velocity (Fig. 8). At low fluid velocities, a relatively thick mass transfer boundary layer (δ) can cause a liquid phase diffusional resistance which decreases substrate concentration at the liquid-biofilm interface and thereby decreases substrate removal rate (Fig. 9).

The experiments reported in this study were conducted at sufficiently high fluid velocities so that liquid phase diffusional resistance was minimized.

Biofilm Accumulation and Shearing Rates

The development of attached biomass is adequately described by a sigmoidal-shaped curve (Fig. 4). The slope of this curve at a particular time is the net biofilm accumulation rate. The variation in the net biofilm accumu-

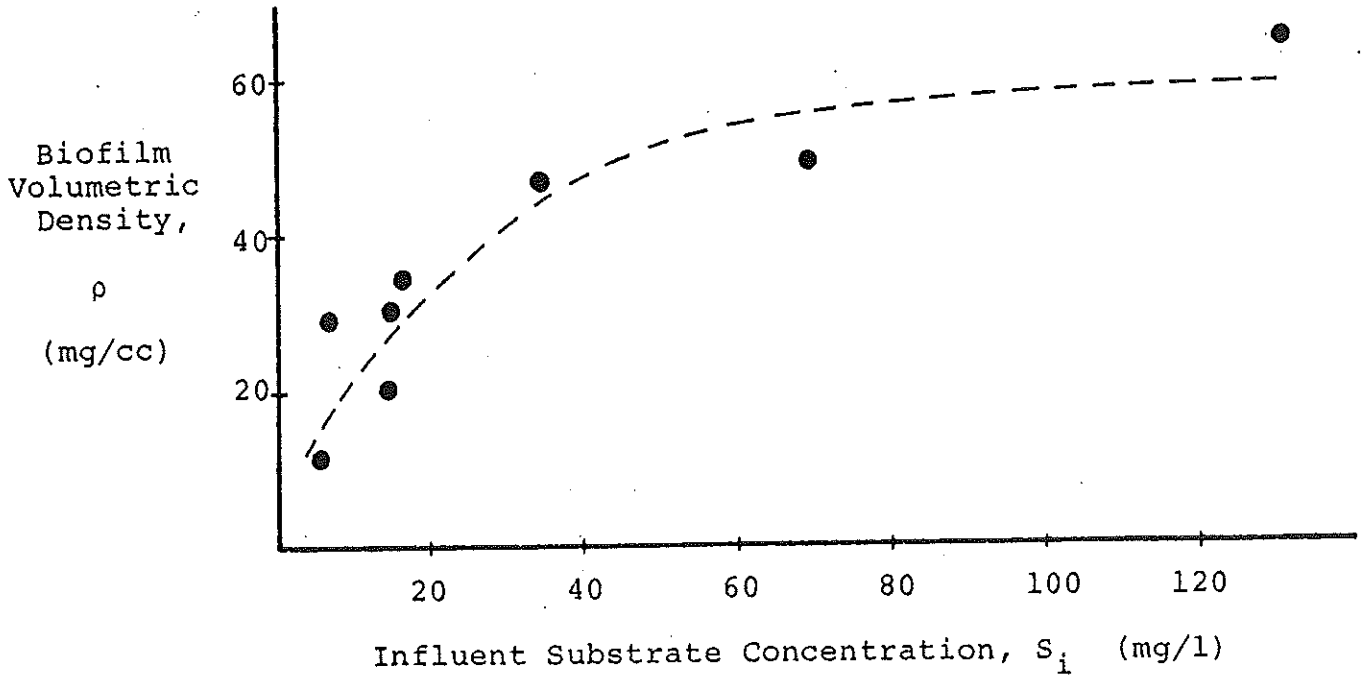

Figure 5. Variation in Biofilm Density with Influent Substrate Concentration

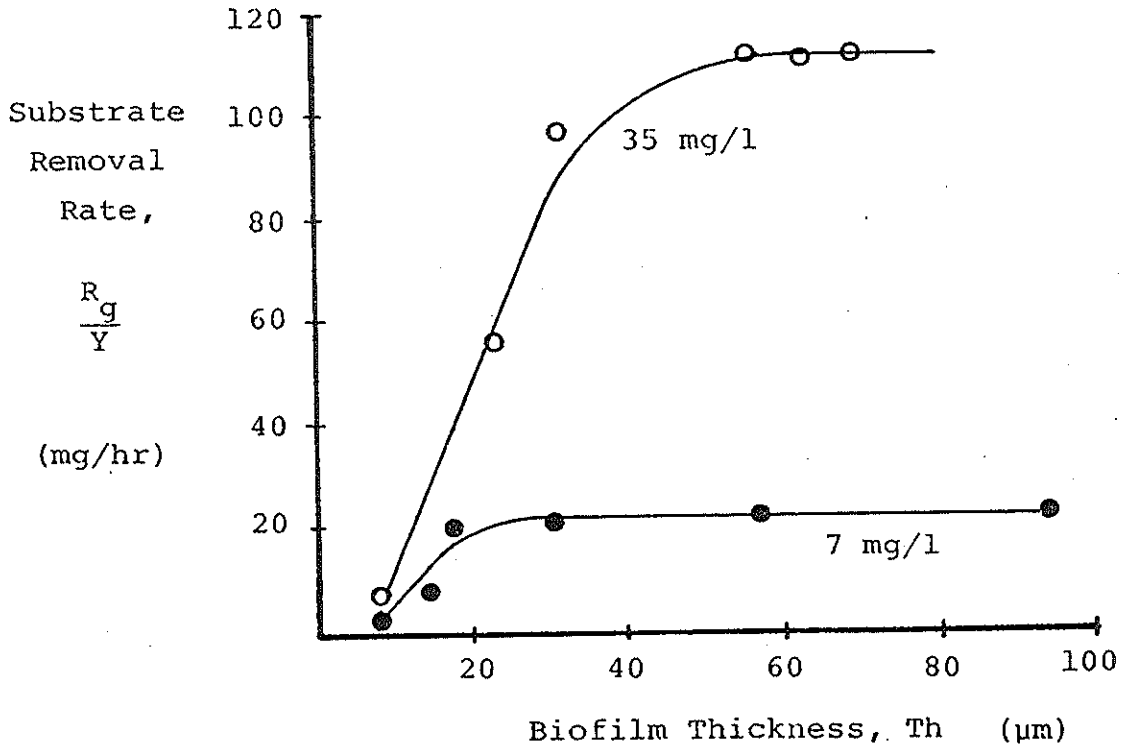

Figure 6. Change in Substrate Removal Rate with Biofilm Thickness

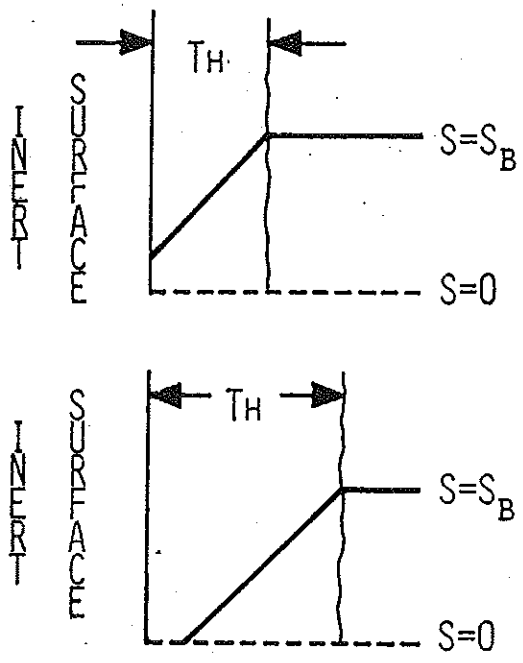

Figure 7. Diffusional Resistances in Biofilms

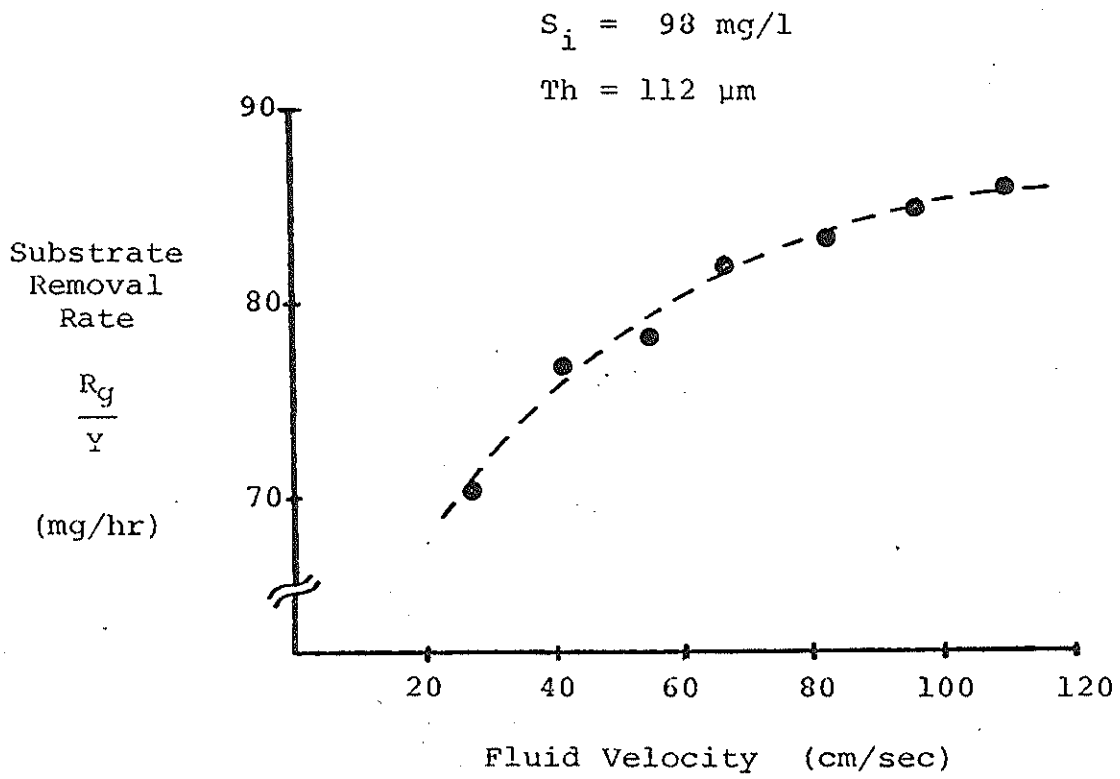

Figure 8. Variation in Substrate Removal Rate with Fluid Velocity

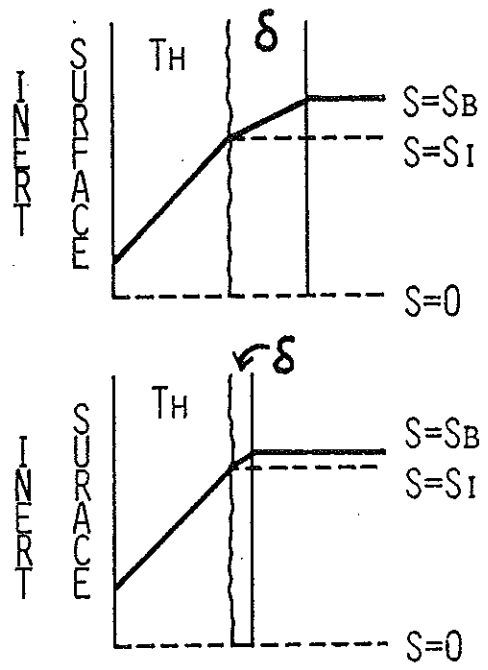

Figure 9. Liquid Phase Resistances

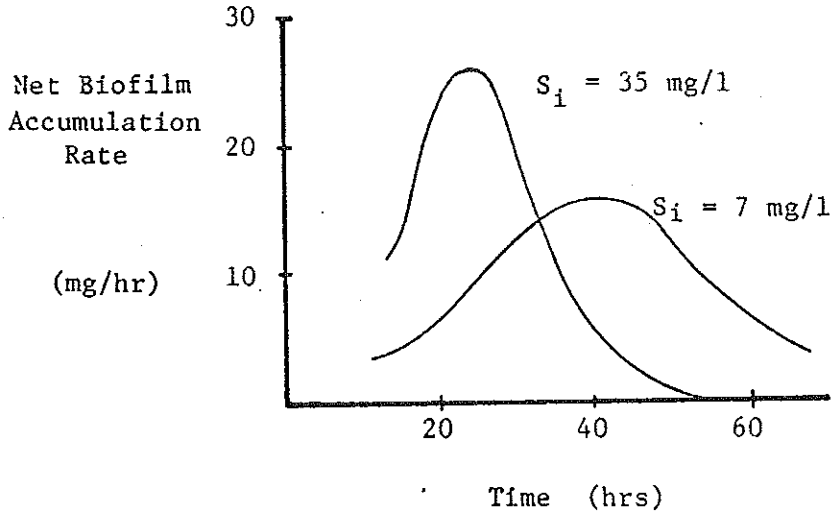

10a.

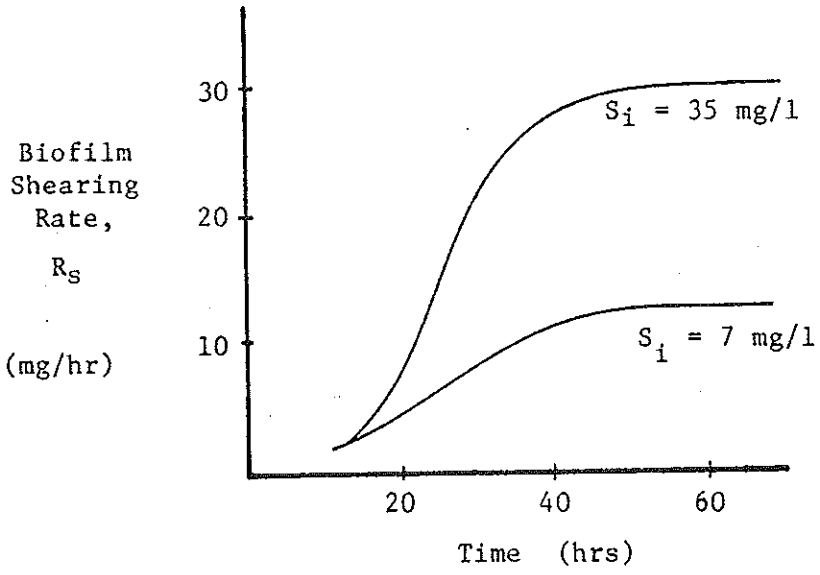

10b.

Figure 10a,b. Change in Biofilm Accumulation and Shearing Rates, Fluid Velocity = 96 cm/sec

lation rate with time is shown in Fig. 10-a for two experiments at different influent substrate concentrations. The rate increases to a maximum value corresponding to the sigmoidal inflection point and then decreases to zero.

The biofilm shearing rate (Fig. 10-b) increases in proportion to the biofilm thickness. The increase in shearing rate with influent substrate concentration is due to a greater biofilm thickness resulting from the higher substrate loading.

Figure 11 indicates the variation in maximum biofilm thickness with influent substrate concentration and fluid velocity. For a given velocity, both the rate of biofilm accumulation (Fig. 10-a) and the maximum accumulation increase with influent substrate concentration.

The effect of fluid velocity on the maximum biofilm thickness and the biofilm shearing rate is illustrated in Figures 11 and 12. An increase in fluid velocity produces a greater shearing rate which results in a decrease of the maximum thickness.

Frictional Resistance in the Tubular Reactor Systems

Increase in fluid frictional resistance due to biofilm accumulation during experiments in which flow rate is maintained constant causes an increase in pressure drop and power requirements for pumping as shown in Fig. 13 for a typical experiment. Conversely, if pressure drop is held constant, flow capacity is reduced. Figure 14 shows a typical experimental curve where flow capacity was reduced to 42% of the original capacity in a 100-hour laboratory experiment. Frictional resistance can be represented for both constant flow rate and constant pressure drop experiments by a dimensionless friction factor given by the following equation:

$$f = 2.0 \frac{d}{L} \frac{\Delta P}{\rho_w \bar{v}^2} \qquad (8)$$

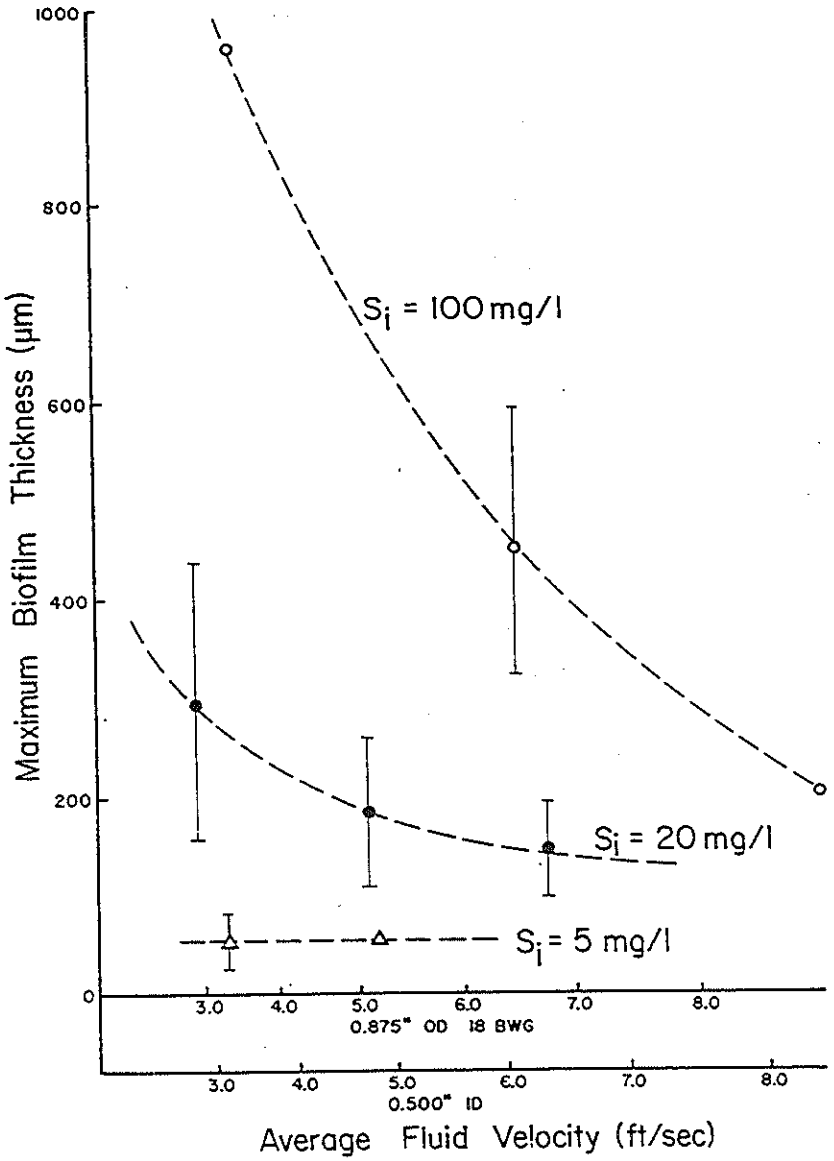

Figure 11. Effect of Substrate Loading and Fluid Velocity on Maximum Biofilm Thickness

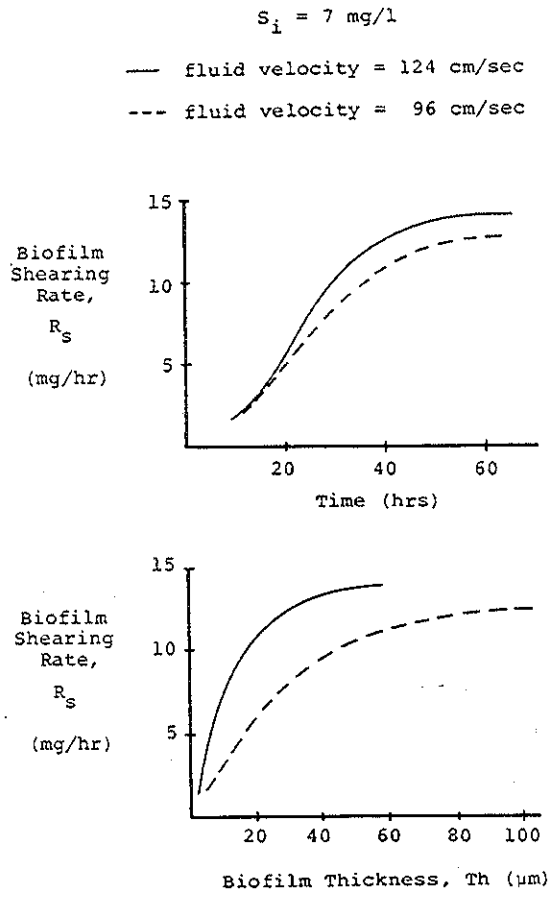

Figure 12. Change in Biofilm Shearing Rate with Time and Biofilm Thickness

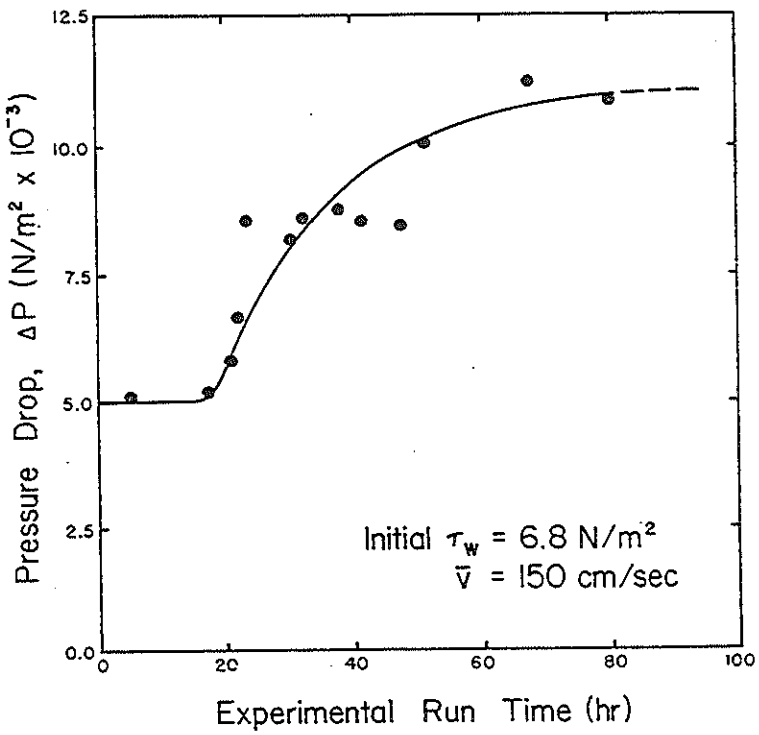

Figure 13. Increase in Pressure Drop During a Constant Flow Rate Experiment

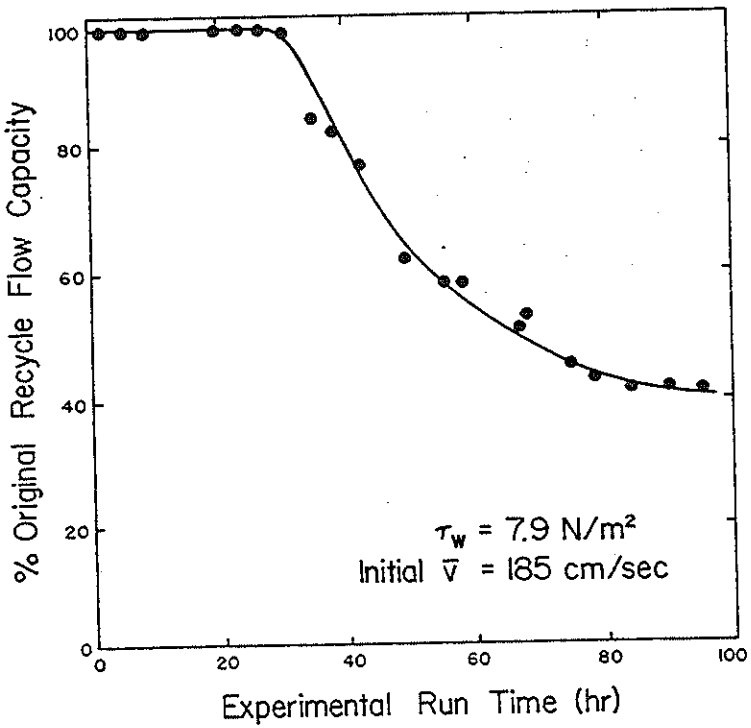

Figure 14. Decrease in Flow Capacity for a Constant Pressure Drop Experiment

where f = friction factor (dimensionless)

d = tube diameter (L)

ρ_w = fluid density (ML^{-3})

$\bar{v}$ = average fluid velocity (Lt^{-1})

ΔP = pressure drop along length L ($ML^{-1}t^{-2}$)

L = length between pressure ports (L)

The change in friction factor with time for a typical experiment is shown in Fig. 15. The measured biofilm thickness for the same experiment is also indicated.

The friction factor is related to the Reynolds number (fluid velocity) and the equivalent sand roughness, k_s, through the empirical Colebrook-White relation. This equation provides good correlation for friction factor vs Reynolds number for various "commercially rough" pipes throughout the hydraulically smooth transition and fully rough regimes. The Colebrook-White equation, solved for the equivalent sand roughness, k_s, yields:

$$k_s = \frac{d}{2}\left[10^{(0.87 - 0.50f^{-\frac{1}{2}})} - \frac{18.70}{Re\ f^{\frac{1}{2}}}\right] \qquad (9)$$

where d = tube diameter (L)

Re = $\bar{v}d/\nu$ = Reynolds number

$\bar{v}$ = mean fluid velocity (L/t)

ν = kinematic viscosity (L^2/t)

This expression can be used to compute an equivalent sand roughness for the biofilm from a measurement of the flow rate and pressure drop.

In all tubular reactor experiments, k_s increases with time; Figure 16 shows the progression of k_s with time for a typical experiment. Figure 17 indicates the dependence of k_s on biofilm thickness for the range of shear stress investigated (6.5 - 7.9 N/m^2). Determination of the flow regime

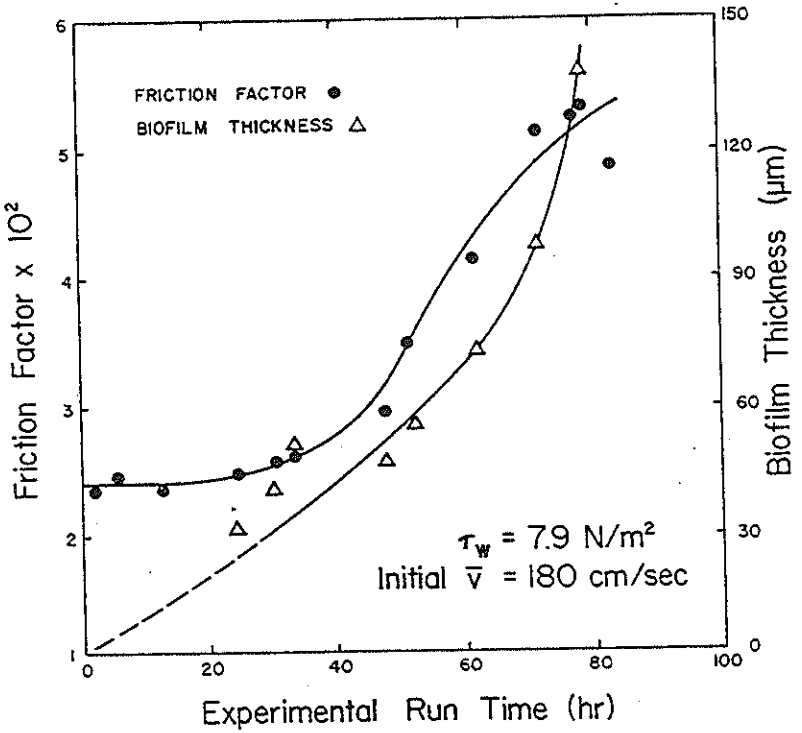

Figure 15. Change in Friction Factor and Biofilm Thickness During a Constant Pressure Drop Experiment

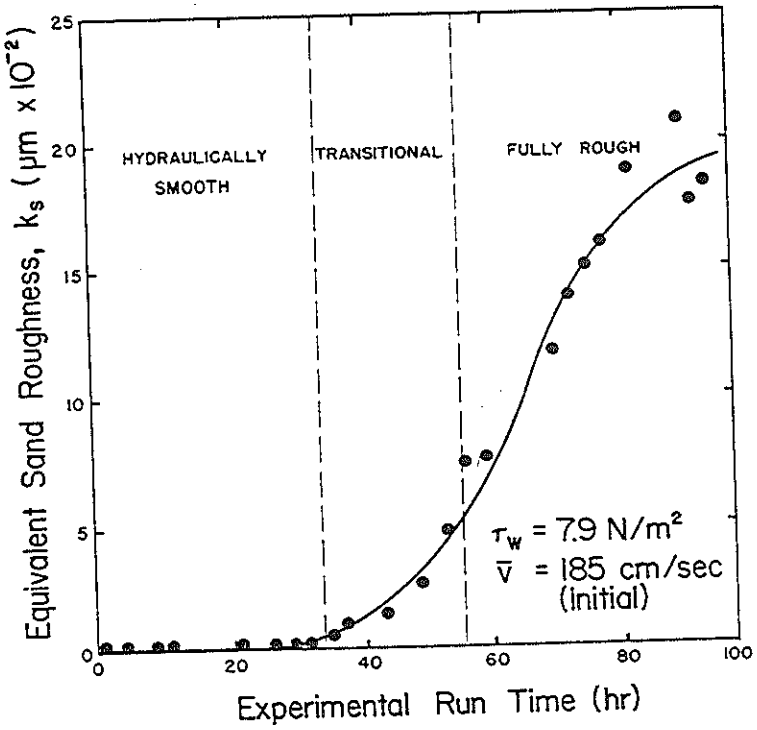

Figure 16. Change in Equivalent Sand Roughness During a Typical Experiment

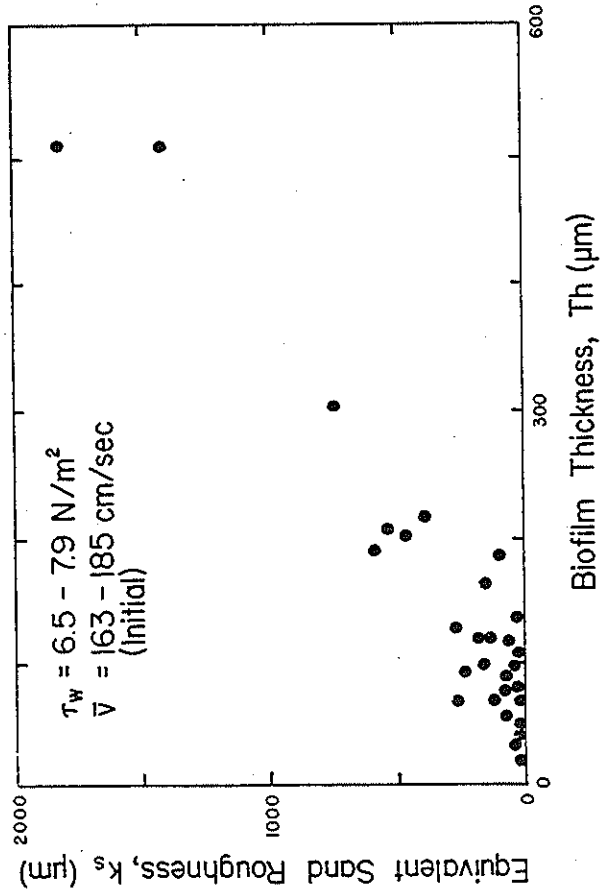

Figure 17. Variation in Equivalent Sand Roughness with Biofilm Thickness

(smooth, transitional or fully rough) depends on the magnitude of k_s relative to the size of the viscous sublayer (δ_1); δ_1 is given by Eq. 10:

$$\delta_1 = \frac{10d}{Re} \left(\frac{f}{2}\right)^{-0.5} \tag{10}$$

When $k_s < \delta_1$, the pipe is considered hydraulically smooth; when $14\delta_1 > k_s > \delta_1$ the flow is in the transitional regime; when $k_s > 14\delta_1$, the flow is in the fully rough regime.[16] In all experiments the flow regime, as determined from the above criteria, progressed from hydraulically smooth to transitional or fully rough.

Frictional resistance of biofilms grown under constant pressure drop have been compared to the frictional resistance of pipes with a rigid roughness as given by the Colebrook-White equation. The following were observed:

1. Frictional resistance due to biofilm development shows a similar dependency on Reynolds number as frictional resistance due to commercially rough pipe surfaces.
2. Frictional resistance is dependent on biofilm thickness.
3. Frictional resistance does not increase above the hydraulically smooth pipe value until a critical biofilm thickness is obtained.

The Blasius-Stanton or Moody diagram[12] can be used to compare frictional resistance due to biofilm development with the frictional resistance of rigid rough surfaces. The Blasius-Stanton diagram is a plot of friction factor vs Reynolds number for a series of pipes with different equivalent sand roughness; the friction factor in a pipe with a rigid rough surface depends on both the relative roughness and the Reynolds number.

The relationship between friction factor and Reynolds number for a constant pressure drop experiment is presented in Figure 18. This figure shows

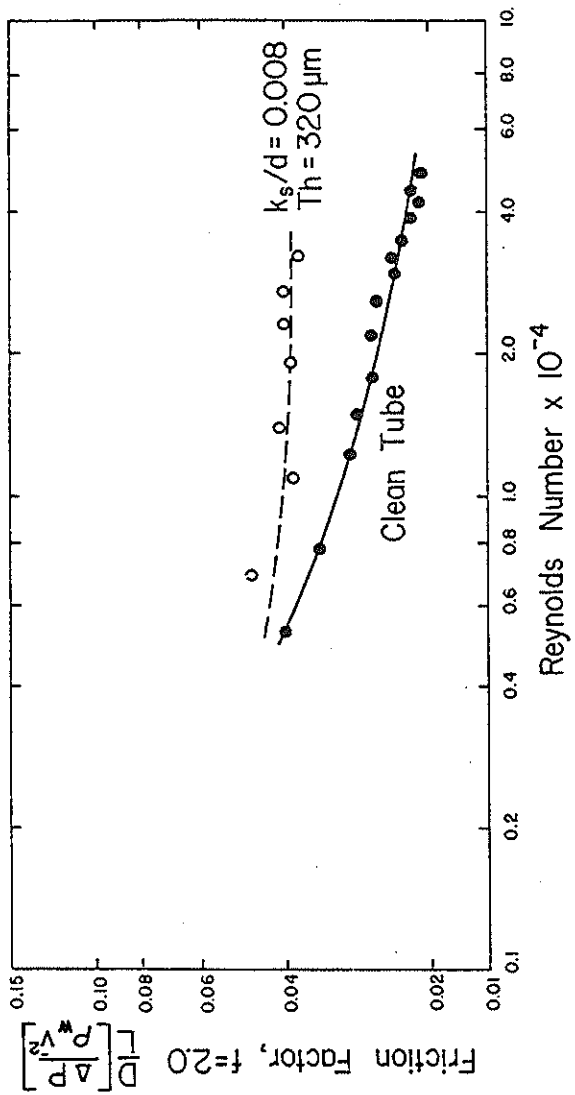

Figure 18. Change in Friction Factor with Reynolds Number for a Clean and Fouled Tube

the dependency of friction factor on Reynolds number is the same as for a tube with a rigid rough surface in the range of Reynolds numbers investigated (5,000 to 48,000). This data was obtained by reducing in steps the fluid velocity from its initial value in a given experiment and calculating friction factor and Reynolds number at each step. Reduction, rather than increase of the velocity from the initial condition minimized shearing of biofilm during the experiment.

Figure 19 shows friction factor vs Reynolds number for an experiment at different stages of biofilm development; friction factor increases with biofilm thickness. The relationship between biofilm thickness and friction factor for all experiments at a wall shear stress from 6.5 - 7.9 N/m^2 is shown in Figure 20. Friction factor is dependent on film thickness after a critical thickness (Th_{crit}) approximately equal to the thickness of the viscous sublayer is attained.

The critical film thickness corresponds to the stage of biofilm development at which surface irregularities protrude through the viscous sublayer. Preceding this stage, the roughness peak is smaller than the viscous sublayer thickness ($k_s < \delta_l$) and friction factor does not increase (the tube is hydraulically smooth). For a wall shear stress of 6.5 - 7.9 N/m^2, the viscous sublayer is approximately equal to 40 micrometers; this compares well with the observed Th_{crit} of 30-35 micrometers for the same wall shear stress range.

Although the frictional resistance effects of biofilm can be adequately described by formulae suitable for rigid rough surfaces, the conclusion should not be drawn that, indeed, the biofilm presents a rigid rough surface to the flow. Such a notion is an oversimplification and cannot account for all experimental observations.[15]

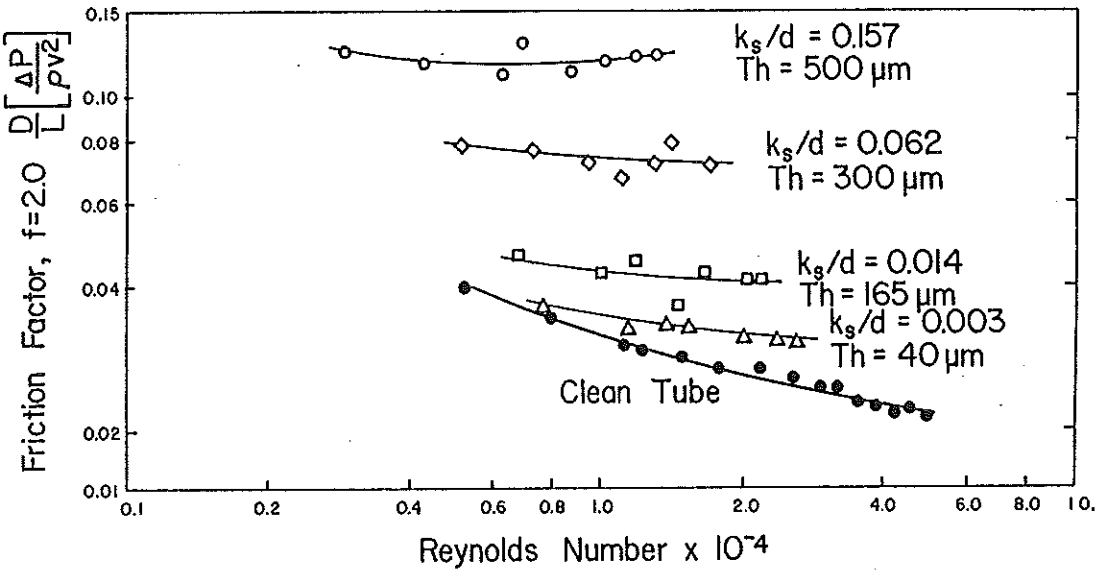

Figure 19. Change in Friction Factor with Reynolds Number During Biofilm Development

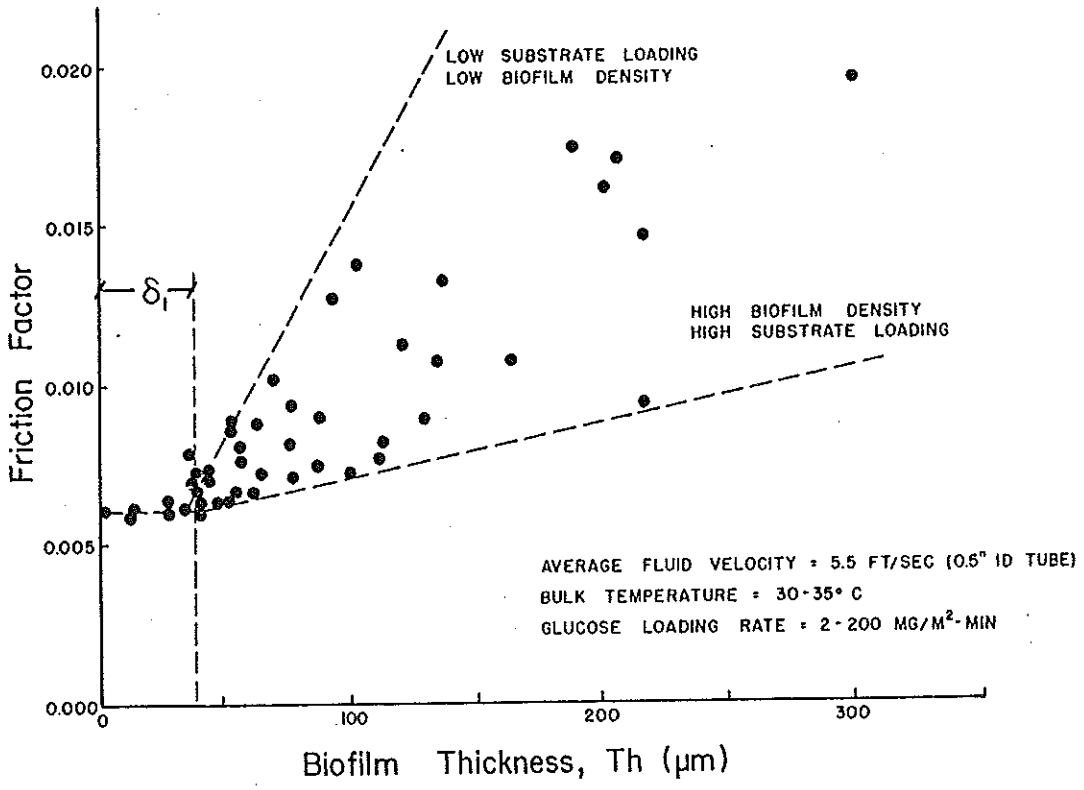

Figure 20. The Effect of Biofilm Thickness on Friction Factor in a Circular Tube

Frictional Resistance in the Annular Reactor System

Increased frictional resistance is also observed in the annular reactor during biofilm development. However, the flow regime, consisting of the superimposition of axial flow (nutrients plus dilution water) through the reactor, centrifugal flow due to the rotating inner cylinder, and circulation induced by the impeller/draft tube arrangement, is too complex for detailed analysis. Fluid dynamic analysis of such a system has not been found in the literature. Some measured fluid dynamic characteristics of the clean reactor are presented in Figure 21.

In the annular reactor, friction factor has been defined as follows:

$$f_a = \frac{T_q}{\pi \rho R_i^3 (R_i + R_o) \Omega^2 H} \qquad (11)$$

where R_i = radius of inner cylinder (L)

R_o = radius of outer cylinder (L)

Ω = rotational velocity (t^{-1})

H = height of inner cylinder (L)

T_q = torque on inner cyliner ($m\text{-}L^2/t^2$)

The change in friction factor during biofilm development for a typical experiment is presented in Figure 22. As in the tubular reactor, biofilm thickness increases before frictional resistance.

Effects on Heat Transfer Resistance

Biofilm development and resulting fluid frictional resistance have been discussed and both influence heat transfer. Changes in heat transfer resistance arise from the combined effects of increased biofilm thickness (conductive heat transfer) and increased frictional resistance (convective heat transfer).

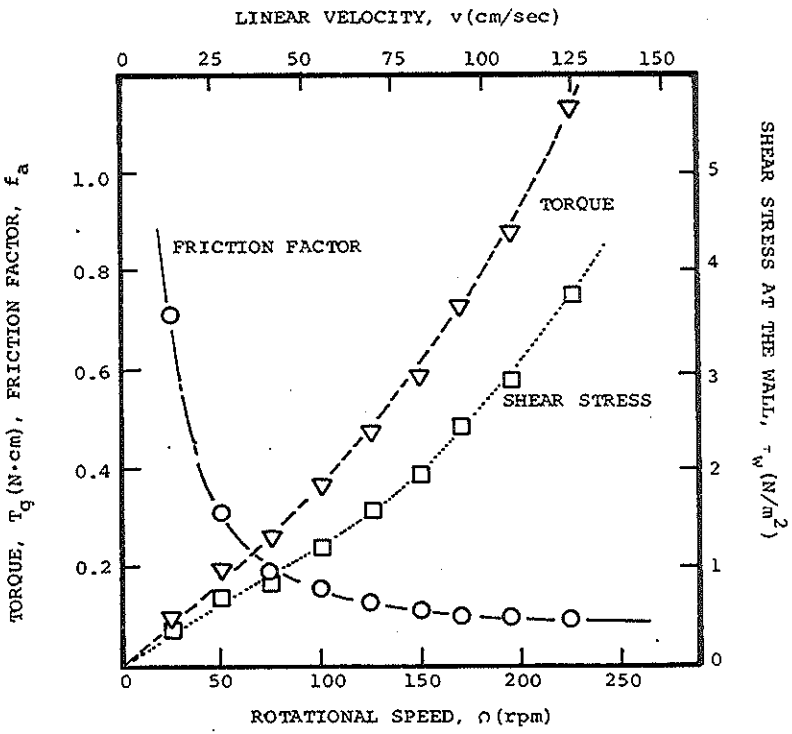

Figure 21. Relevant Fluid Dynamic Characteristics of the Clean Annular Reactor System at 30°C

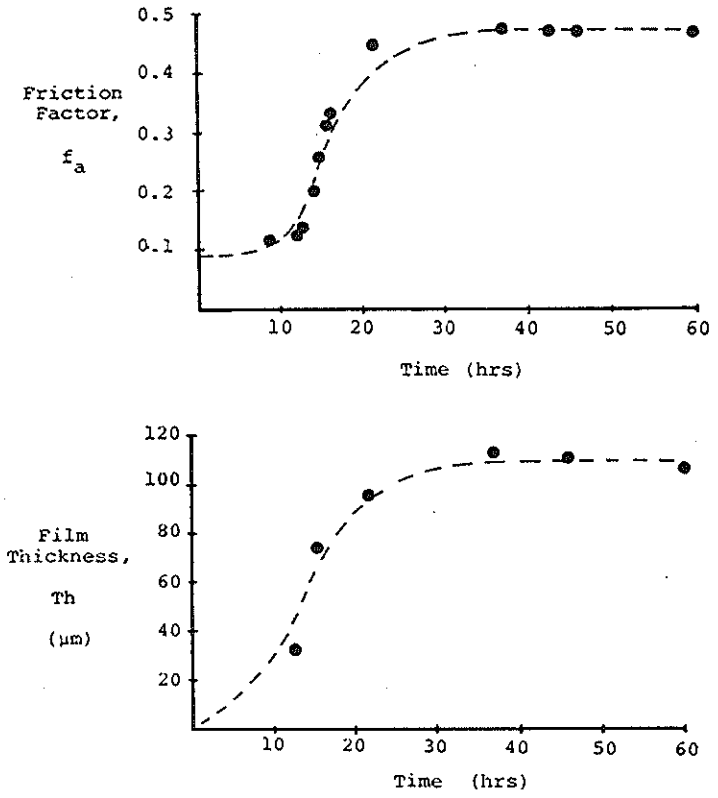

Figure 22. Change in Friction Factor and Biofilm Thickness During an Annular Reactor Experiment

Conductive heat transfer can be related to biofilm thickness and its effective thermal conductivity. Experimental biofilm thermal conductivity determinations indicate no significant difference from that of water at the same temperature (Table 1). This is not surprising since biofilm is approximately 98-99% water.

Convective heat transfer results from fluid mixing or motion, and can be related to momentum transfer or frictional resistance. Colburn[7] correlated convective heat transfer in tubes to friction factor and properties of the fluid. The Colburn relationship is only useful when the biofilm is thicker than the viscous sublayer.

Overall heat transfer resistance due to biofouling film development can then be calculated if the following are known:

1. Biofilm thickness and thermal conductivity
2. Frictional resistance
3. Wall temperature and bulk temperature

Figure 23 describes a typical experiment in the laboratory heat exchange reactor and illustrates the relative effects of conductive and convective heat transfer resistance on overall heat transfer resistance.

Biofilm Destruction by Chemical Oxidants

Chlorination is the most common method used for controlling fouling biofilm development. Therefore, an attempt to further define the chlorine-biofilm reaction was included in this study. Other chemical oxidants were tested in a limited number of experiments. The major concerns were as follows:

1. rate of chlorine consumption by biofilms
2. rate of biofilm destruction by chlorine
3. chlorine demand of biofilm (stoichiometry)
4. regrowth of biofilm subsequent to chlorination

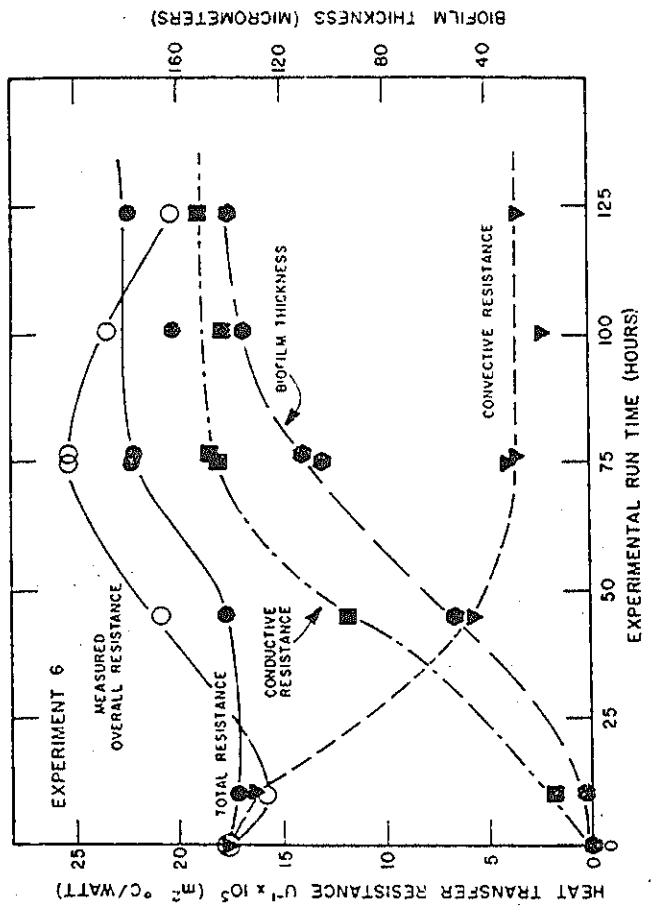

Figure 23. Changes in Heat Transfer Resistance as a Result of Biofilm Accumulation

TABLE 1. Thermal Conductivity of Biofilms [14]

Expt.	Input Glucose Conc. (mg/l)	Biofilm Thermal Conductivity watt/m°C	Bulk Temperature °C
1	100	0.70 ± 0.40 (3)	31.89 ± 0.49
2	10	0.71 ± 0.10 (3)	31.50 ± 0.03
6	10	0.68 ± 0.22 (5)	28.30 ± 0.03
7	25	0.52 ± 0.21 (3)	26.70 ± 0.03
8	10	0.70 ± 0.38 (5)	26.70 ± 0.03
9	10	0.58 ± 0.14 (5)	28.30 ± 0.03
	GRAND MEAN:	0.65 ± 0.24 (24)	
	Water	0.61	26.7
	Water	0.62	32.2

Batch experiments were conducted primarily in a tubular reactor under turbulent flow conditions with "mature" biofilms. Some continuous flow experiments were conducted in the annular fouling reactor.

The results of these experiments, and continuing research in our laboratories, are applicable to biofouling film destruction. However, since our methods are directed toward elucidation of process rates within the biofilm, the results may be equally relevant to other microbial aggregates, such as those found in water and wastewater treatment effluents.

Rate of Chlorine Consumption by Biofilms

Batch experiments were initiated by injecting a pulse of chlorine into the recycle section of the tubular reactor and observing the disappearance of chlorine (actually, total oxidant). The input pulse invariably resulted in an exponential decrease of chlorine, as illustrated in Figure 24, for seven successive injections of equal magnitude. Chlorine disappearance rate for an individual injection can be described as follows in a batch reactor:

$$V \frac{d[OX]}{dt} = -k_1 A_s [OX] \qquad (12)$$

where [OX] = chlorine concentration (ML^{-3})

A_s = reactor surface area covered by biofilm (L^2)

V = reactor volume (L^3)

k_1 = process rate coefficient (Lt^{-1})

t = reaction time (t)

k_1 has units of velocity (Lt^{-1}) or a surface rate coefficient since the reaction is occurring at the water/biofilm interface. Figure 24 indicates that each successive injection resulted in a decreasing k_1 for a given biofilm.

The first order rate expression (Eq. 12) may be indicative of a first order reaction or a mass transfer limitation occurring in the bulk fluid or

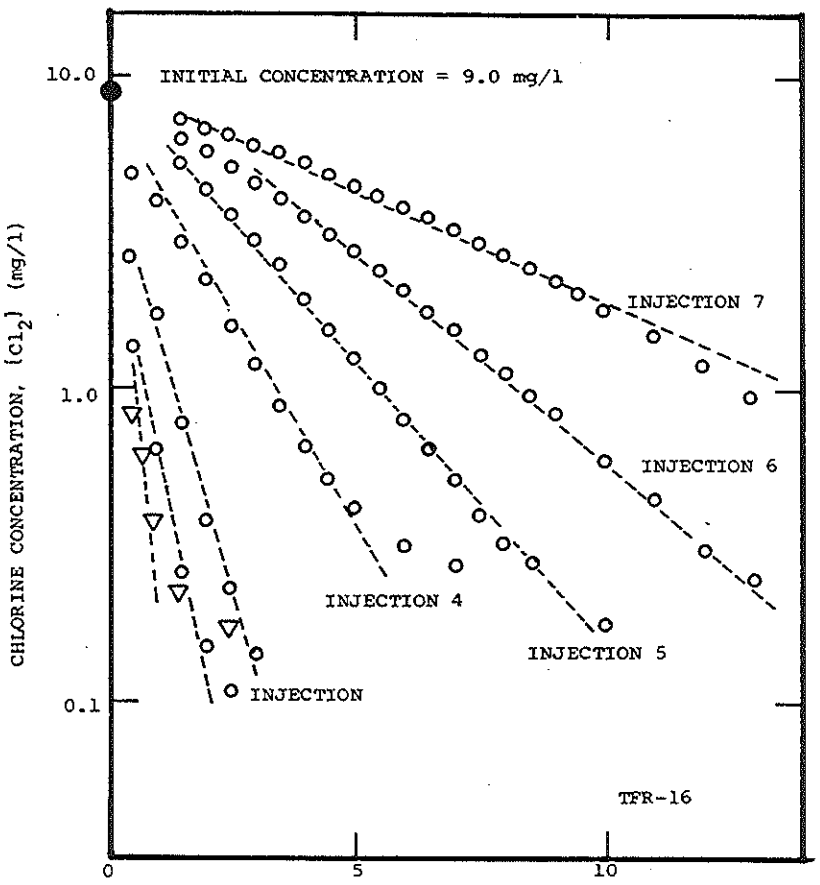

Figure 24. Chlorine Decay Due to Reaction with Biofilm for Seven Consecutive Injections in the Tubular Reactor System

within the biofilm. The potential for diffusion limitation in the biofilm appears reasonable since chlorine is extremely reactive in the biofilm.

Biofilm Destruction

Biofilm destruction rates could not be directly determined because the biofilm sampling techniques used were not amenable for use during chlorination tests. Therefore, biofilm thickness data are restricted to before and after chlorination. However, biofilm destruction rates were indirectly monitored during chlorination by pressure drop measurements or torque measurement. Figures 25 and 26 illustrate changes in pressure drop and torque for typical experiments as a function of chlorine reacted.

Biofilm destruction due to chlorine addition is evident. Figure 27 illustrates the increase in organic carbon concentration in a continuous flow, annular reactor experiment following a pulse injection of chlorine. Organic carbon increased from 1 mg/l prior to treatment to 6.5 mg/l before decreasing to 3 mg/l after 45 minutes. The organic carbon wasted in the effluent reflects the removal of approximately 45.3 mg of biofilm or about 10 μm of biofilm for this particular experiment.

Results indicate that chlorine attacks the extracellular polymers which maintain the integrity of the biofilm matrix. Chlorine causes depolymerization resulting in removal of the weakened biofilm matrix by fluid shear stress. Continued biofilm removal is frequently observed even when all chlorine is dissipated which implies the important role of fluid shear stress in the overall biofilm destruction process. Norrman[13] also recorded the enhancing effect of fluid shear stress on biofilm destruction by chlorination. The results suggest the following progression for biofilm destruction by chlorine:

1. chlorine is transported from the bulk fluid to the biofilm
2. chlorine penetrates into the biofilm reacting with binding polymers

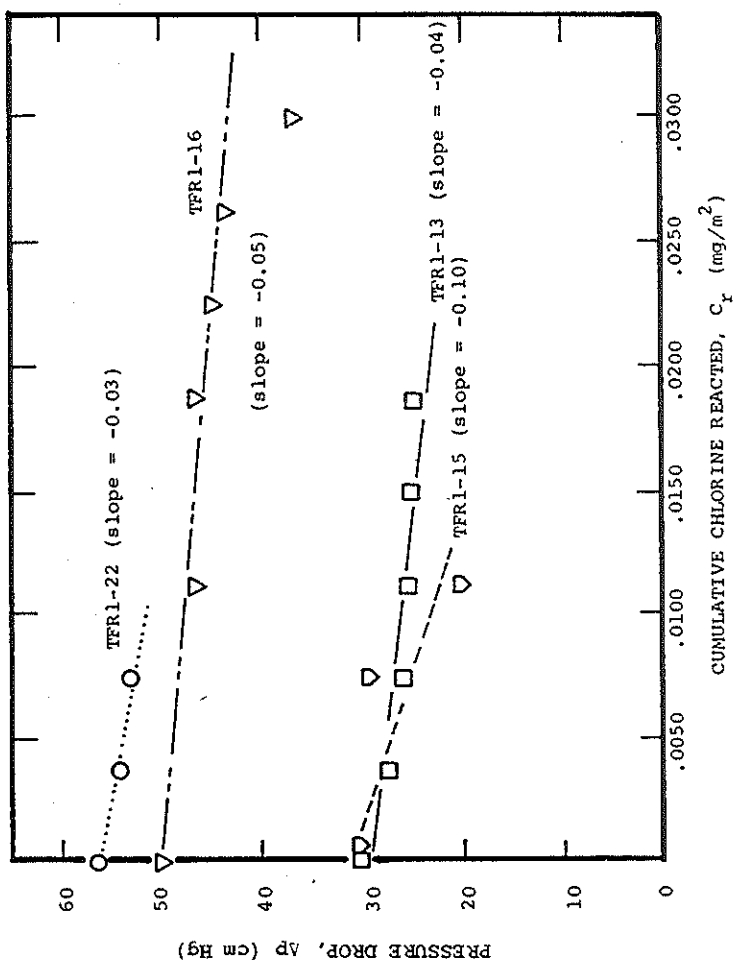

Figure 25. Change in Pressure Drop Due to Treatment of Biofilm with Chlorine in the Tubular Reactor System

4. Biofilm development results in energy losses. Specifically, biofilms contribute to fluid frictional losses and heat transfer losses.
5. Beyond a "critical" thickness, biofilm accumulation may create large increases in fluid frictional resistance. The "critical" biofilm thickness, observed experimentally, compares favorably with the viscous sublayer thickness calculated for flow in the clean tube.
6. The increase in friction factor due to biofilms can be described by the traditional "equivalent sand roughness" concept, even though the mechanism of energy dissipation is much more complex.
7. Changes in overall heat transfer resistance arise from the combined effect of biofilm development on both conductive and convective heat transfer.
8. Chlorine reaction with biofilm is approximately first order with respect to chlorine concentration, probably a result of diffusional limitation in the biofilm.
9. Biofilm destruction by chlorine is a result of oxidation of portions of the biofilm which weakens the film structure and results in partial removal by fluid shear.
10. Biofilm development can be more rapid following chlorine treatment. Since biofilm destruction is seldom complete, the residual deposit appears to catalyze "regrowth."

ACKNOWLEDGMENTS

The authors gratefully acknowledge the following: 1) the Electric Power Research Institute (RP902-1) and the National Science Foundation (ENG 74-11957 and ENG 77-26934) for partial financial support; 2) Drs. B.F. Picologlou and L.V. McIntire for significant contributions to the experimental program; 3) Dr. Willi Gujer for his advice and valuable comments concerning data analysis; and 4) Linda Graetz and Maurine Lee for manuscript preparation.

REFERENCES

1. Atkinson, B. Biochemical Reactors, Pion Ltd., London (1974).
2. Baier, R. E. "Applied Chemistry at Protein Interfaces," Adv. Chem. Series, #145, American Chemical Society, p. 1, (1973).
3. Baier, R. E. "Influence of the Initial Surface Condition of Materials on Bioadhesion," Proc. 3rd Int'l. Cong. on Marine Corrosion and Biofouling, Gaithersburg, MD. (1972).
4. Baier, E. E. and V. A. Depalma. "Microfouling of Metallic and Coated Metallic Flow Surfaces in Model Heat Exchanger Cells," Calspan Corp. Report, Buffalo, N.Y. (1977).
5. Baier, R. E., E. G. Shafin, and W. A. Zisman, "Adhesion: Mechanisms that Assist or Impede It," Science, Vol. 162, No. 2, p. 1360, (1968).
6. Characklis, W. G. "Biofilm Development and Destruction," Final Report, Electric Power Research Institute RP 902-1, Palo Alto, CA. (1979).
7. Colburn, A. P. "Correlation of Momentum and Energy Transfer," Trans. A.I.Ch.E., Vol. 29, pp. 174-210, (1933).
8. Harremoes, P. "Half-order Reactions in Biofilm Kinetics," Vatten, Vol. 2, pp. 122-143, (1977).
9. Kornegay, B. H. and J. F. Andrews. "Characteristics and Kinetics of Biological Film Reactors," Final Report, Federal Water Pollution Control Administration, Research Grant WP-01181l, Dept. Environmental Systems Engineering, Clemson University, Clemson, S.C. (1967).
10. LaMotta, E. J. "Evaluation of Diffusional Resistances in Substrate Utilization by Biological Films," Ph.D. Dissertation, University of North Carolina at Chapel Hill (1974).
11. Marshall, K. C., R. Stout, and R. Mitchell. "Mechanism of the Initial Events in the Sorption of Marine Bacteria to Surfaces, J. Gen. Microbiol., Vol. 68, pp. 337-348, (1971).

12. Moody, L. F. "Friction Factor Dependency on Reynolds Number and Pipe Roughness," Trans. ASME, Vol. 66, No. 671, (1944).

13. Norrman, G. "Control of Microbial Fouling in Circular Tubes with Chlorine," M.S. Thesis, Dept. Environmental Science & Engr., Rice University, Houston, Tx. (1976).

14. Nimmons, M. J. "Biofilm Effects on Heat Transfer Resistances within a Turbulent Flow System," M.S. Thesis, Dept. Environmental Science & Engr., Rice University, Houston, Tx. (1979).

15. Picologlou, B., N. Zelver, and W. G. Characklis. "Influences of Biofilms on Hydraulic Deterioration in Circular Tubes," submitted for publication: J. Hydraulics Div., ASCE, (1979).

16. Schlichting, H. Boundary Layer Theory, 6th edition, McGraw-Hill, N.Y. (1968).

17. Zelver, N. "Biofilm Development and Associated Energy Losses in Water Conduits," M.S. Thesis, Dept. Environmental Science & Engr., Rice University, Houston, Tx. (1979).

18. Zobell, C. E. "The Effects of Solid Surfaces Upon Bacterial Activity," J. Bact., Vol. 46, pp. 39-56, (1943).